Macromolecules
COMMUNICATION TO THE EDITOR

Macromolecules **2010**, *43*, 7891–7894 **7891**
DOI: 10.1021/ma101655s

Field-Effect Carrier Transport in Poly(3-alkylthiophene) Nanofiber Networks and Isolated Nanofibers

Sadaki Samitsu,*,† Takeshi Shimomura,‡ Seiji Heike,§ Tomihiro Hashizume,§,∥,⊥ and Kohzo Ito*,#

†*Functional Thin Films Group, Organic Nanomaterials Center, National Institute of Materials Science, 1-1 Namiki, Tukuba 305-0044, Japan,* ‡*Tokyo University of Agriculture and Technology, Nakamachi 2-24-16, Koganei-shi, Tokyo 184-8588, Japan,* §*Advanced Research Laboratory, Hitachi, Ltd., Hatoyama 350-0395, Japan,* ∥*Department of Physics, Tokyo Institute of Technology, Meguro 152-8550, Japan,* ⊥*WPI Advanced Institute for Materials Research, Tohoku University, Sendai 980-8577, Japan, and* #*Department of Advanced Materials Science, Graduate School of Frontier Sciences, The University of Tokyo, 5-1-5-603 Kashiwanoha, Kashiwa, Chiba 277-8561, Japan*

Received July 27, 2010
Revised Manuscript Received September 2, 2010

Application of one-dimensional nanostructures such as nanofibers and nanowires is a promising strategy for improving the device performance of organic thin film transistors.[1] This is because these nanostructures enable the device dimensions to be reduced without the use of the costly optical lithography techniques currently employed in industrial silicon technology. Solution-processable nanofibers consisting of polythiophenes have great potential as the active layer of a printable transistor and have thus been prepared by a variety of procedures.[2] In particular, the whisker method offers industrial advantages as it allows the simple mass production of high-quality semicrystalline nanofibers.[3] Several studies have reported the field-effect carrier transport of nanofibers of poly(3-hexylthiophene) (P3HT), where carrier mobilities as high as 0.1 $cm^2/(V\ s)$ and on/off ratios above 10^6 have been obtained.[4] However, there have been no reports on the effect of alkyl chain length on the carrier transport of poly(3-alkylthiophene) (P3AT) nanofibers, which should be of considerable interest because previous studies have revealed that alkyl chain length has a large influence on device performance of P3AT thin-film transistors. Longer alkyl chains in P3AT thin film have dramatically reduced the field-effect mobility.[5] On the basis of the whisker method using selected solvents, we have achieved effective and highly reproducible production of nanofibers composed of four P3ATs substituted with *n*-butyl, *n*-hexyl, *n*-octyl, and *n*-decyl side chains.[3c−e] The resulting nanofibers consist of periodic stacks of extended polymer backbones along the fiber direction and two-three laminated layers of the polymer stacks separated by alkyl side chains normal to the fiber direction. The cross-section is 3−4 nm in height and 24−27 nm in width, both dimensions increasing slightly with the alkyl chain length (Figure S1 in the Supporting Information). A nanofiber length of several micrometers represents a high aspect ratio of 100−1000. This successful step helps to elucidate crucial factors that dominate the device performance of the P3AT-nanofiber transistor. Very recently, Oosterbaan et al. have reported field-effect mobility of P3AT nanofiber films (30−80 nm in thickness), which values are $2.4-3.5 \times 10^{-3}$ $cm^2/(V\ s)$ irrespective of alkyl-side-chain length.[6] Here, we investigate the field-effect carrier transport of P3AT nanofibers (∼3−4 nm in thickness), focusing on alkyl chain length dependence (four to eight carbon atoms in the side chains) and nanofiber geometry, i.e., nanofiber network vs isolated nanofibers. We use the same solvent (a solvent mixture of anisole and chloroform) for nanofiber fabrication in contrast to the Oosterbaan case selecting different solvents (*o*-chlorotoluene, *p*-xylene, and pinane) depending on alkyl chain length of P3AT.

P3AT (0.050 wt % P3AT) was dissolved in a solvent mixture of anisole/chloroform (4:1 v%) by heating above 70 °C. The solution was then gradually cooled to 20 °C at a constant rate of 25 °C/h. Orange solutions of P3AT turned brown (P3BT) or purple (P3HT, P3OT, and P3DT) due to the formation of nanofibers.[3c] The nanofiber solution was spin-coated on a silicon substrate with wide-gap electrodes (36 μm). The nanofibers formed a dense network between the electrodes (Figure 1a). It is noted that the concentration of the solution was 10−20 times lower than the concentration of the standard solution used for fabrication of a P3AT thin-film transistor.[5] Despite the low concentration, the surface between the electrodes was mostly overlaid by the nanofiber, and the corresponding surface coverage was determined to be 70−80%, irrespective of the alkyl chain length of P3AT. The thickness of the nanofiber network was roughly as small as the height of the nanofiber (∼4 nm). The channel layer of the nanofiber transistor is much thinner than that of a conventional thin-film transistor, which is several tens of nanometers.[5] This small thickness enables AFM to directly reveal the self-organized structure of P3AT in the channel layer effective for device operation and to shed light on the relation between charge transport and morphology.

We measured the field-effect carrier transport of the nanofiber network at 290 K using a bottom gate configuration. The source-drain current−voltage I_D-V_D characteristics exhibited marked amplification of I_D with respect to the negative gate voltage V_G, leading to an $I_D \sim -0.5\ \mu A$ at a V_D of −30 V and a V_G of −30 V (Figure 1b). I_D increases linearly at a low negative V_D of −5 V and clearly saturated at a high V_D of −30 V. The device operation at a V_D of −5 and −30 V corresponds, respectively, to a linear and saturation regime (see the Supporting Information, Figure S2). The field-effect transistor of the nanofiber network was operated by injected holes, and the nanofibers behaved as a p-type semiconductor. Table 1 summarizes typical parameters that characterize the field-effect carrier transport in the nanofiber network, such as mobility in the linear regime μ_{linear}, mobility in the saturation regime μ_{sat}, threshold voltage V_T, turn-on voltage V_{ON}, and on−off ratio I_{ON}/I_{OFF}. For each nanofiber network, μ_{linear} is comparable to the respective μ_{sat} within a 20% variation, suggesting that there was little influence of contact resistance in device operations.

As compared with the P3HT nanofiber reported previously, the field-effect mobility of the P3HT nanofiber network is slightly smaller than the higher values (1.2×10^{-1} $cm^2/(V\ s)$,[4c] 6.0×10^{-2} $cm^2/(V\ s)$,[4a] and 4.0×10^{-2} $cm^2/(V\ s)$[4d]) but comparable to the lower values (2.0×10^{-2} $cm^2/(V\ s)$,[4b] 1.4×10^{-2} $cm^2/(V\ s)$,[4g] 1.2×10^{-2} $cm^2/(V\ s)$,[3g] and 1.0×10^{-2} $cm^2/(V\ s)$[4e,f]). Despite the wide variety of preparation conditions, such as the casting solvent, temperature step, and casting methods, the nanofibrous structure of P3HT gives a high field-effect mobility owing to the well-organized microstructure of P3HT.

*To whom correspondence should be addressed. E-mail: SAMITSU.Sadaki@nims.go.jp (S.S.); kohzo@k.u-tokyo.ac.jp (K.I.).

Published on Web 09/13/2010

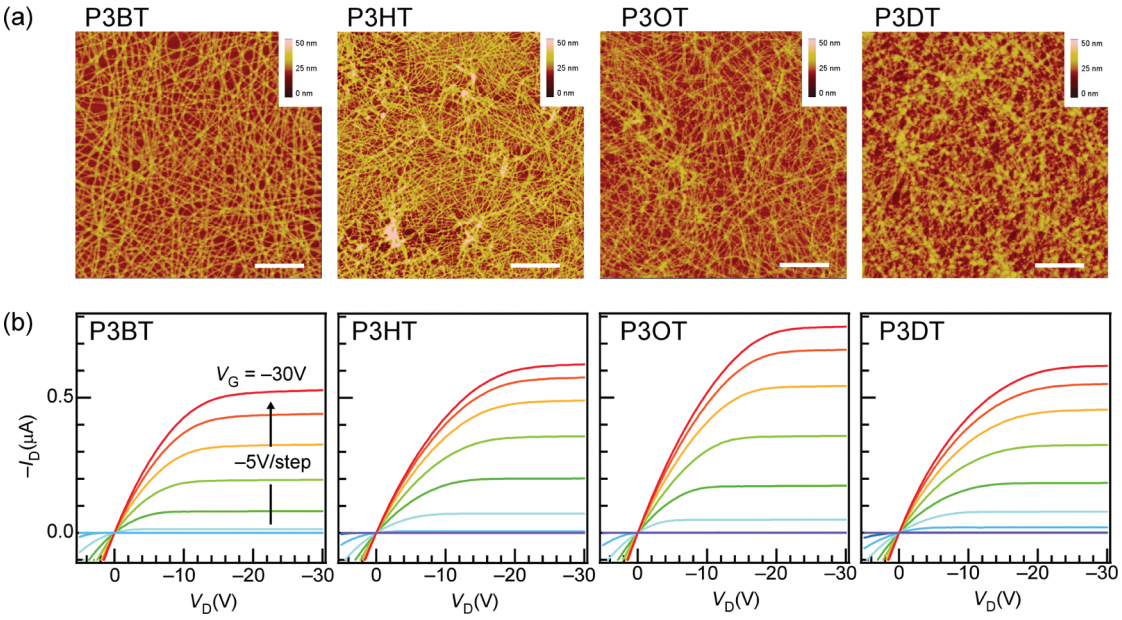

Figure 1. (a) Network morphologies of P3AT nanofiber (scale bar, 1 μm). (b) Field-effect I_D-V_D characteristics of the nanofiber network transistor operated in the V_G range +5 to −30 V at 290 K.

Table 1. Field-Effect Transistor Characteristics of Nanofiber Networks

	linear[a]				saturation[b]			
P3AT	μ_{linear} (cm^2/s)	V_T (V)	V_{ON} (V)	I_{ON}/I_{OFF}	μ_{sat} (cm^2/s)	V_T (V)	V_{ON} (V)	I_{ON}/I_{OFF}
P3BT	1.6×10^{-2}	−13.3	−8	2×10^4	1.7×10^{-2}	−10.4	−7	5×10^4
P3HT	9.8×10^{-3}	−7.3	−1	2×10^4	1.1×10^{-2}	−5.2	−1	5×10^4
P3OT	1.2×10^{-2}	−9.5	−6	2×10^4	1.4×10^{-2}	−7.4	−6	8×10^4
P3DT	1.3×10^{-2}	−12.0	−2	2×10^4	1.1×10^{-2}	−6.7	−2	4×10^4

[a] Field-effect mobility μ_{linear} was determined by eq 1) in a linear regime ($V_D = -5$ V). [b] Field-effect mobility μ_{sat} was determined by eq 2 in a saturation regime ($V_D = -30$ V).

$$I_D = \frac{W^{ef}_{two}}{L_{two}} C_{ox}\mu_{linear} V_D(V_G - V_T) \quad (1)$$

$$I_D = \frac{W^{ef}_{two}}{2L_{two}} C_{ox}\mu_{sat}(V_G - V_T)^2 \quad (2)$$

V_T is the threshold voltage, C_{ox} is the capacitance per unit area of the insulating layer, L_{two} is the electrode spacing, ϕ is the surface coverage of the nanofiber, W_{two} is the nominal width of the two-probe electrode; the effective width of the two-probe electrode is $W^{ef}_{two} = W_{two}\phi$. V_{ON} is the turn-on voltage below which the absolute value of I_D increases rapidly with increasing negative V_G. See Figure S2 in the Supporting Information.

Several researchers have studied the effect of the alkyl chain length of P3AT and reported the following field-effect mobilities for thin-film devices: 1.0−3.0 × 10^{-2} cm^2/(V s) for P3HT and 10^{-6} cm^2/(V s) for P3DT;[5a] 1.0 × 10^{-2} cm^2/(V s) for P3BT, 2.9 × 10^{-3} cm^2/(V s) for P3HT, and 9.1 × 10^{-4} cm^2/(V s) for P3DT;[5b] 1.2 × 10^{-3} cm^2/(V s) for P3BT, 1.0 × 10^{-2} cm^2/(V s) for P3HT, 2.0 × 10^{-4} cm^2/(V s) for P3OT, and 6.6 × 10^{-5} cm^2/(V s) for P3DT;[5c,d] 1.4 × 10^{-2} cm^2/(V s) for P3HT and 1.3 × 10^{-3} cm^2/(V s) for P3OT;[5e] 1.0 × 10^{-2} cm^2/(V s) for P3BT, 5.4 × 10^{-3} cm^2/(V s) for P3HT, and 5.2 × 10^{-4} cm^2/(V s) for P3OT.[5f] All the values listed here clearly show the significant influence of the alkyl chain length on the field-effect mobility. The longer alkyl chain of P3AT dramatically decreases the mobility in the thin-film devices. Surprisingly, however, the nanofiber networks investigated here show little influence of alkyl chain length and all nanofiber devices give a high mobility of ~0.01 cm^2/(V s), even for P3OT and P3DT (Table 1). Nanofiber devices consisting of P3OT and P3DT yield mobilities 1 to 2 orders of magnitude higher than thin-film devices, whereas those consisting of P3BT and P3HT show a mobility comparable to or an order of magnitude larger than thin-film devices. Compared with a thin-film device, a nanofiber network improves device performance, particularly in the case of P3AT with its longer alkyl chains (P3OT and P3DT). The high mobility of nanofiber devices irrespective of alkyl chain length results from the well-ordered stacks of fully extended P3AT backbones in the nanofibers.[3c] Thus, the dramatic decrease in the mobility of P3OT and P3DT thin films reported previously may be attributed not to the inherent character of the P3AT polymer but rather to the self-assembled microstructure of the polymer chains. In a typical device fabrication method, P3AT molecules dissolved in a solvent are cast on a substrate and form thin films through evaporation of the solvent. Evaporation of the solvent leads to self-organization of P3AT when the concentration exceeds the saturation concentration. The self-organization kinetics can be greatly affected by the alkyl chain length, a major determining factor in the solubility and aggregation behavior of P3AT. Longer alkyl chains yield a higher solubility (i.e., saturation concentration), leading to self-organization from a higher concentration.[3c] Many studies have reported on the variation of device performance with deposition conditions.[4c,e,7] The kinetics of P3AT self-assembly is also affected by film thickness because the thinner the film, the shorter the time to complete solvent evaporation. In the case of relatively thick films (several tens of nanometers), solvent evaporation on a substrate is

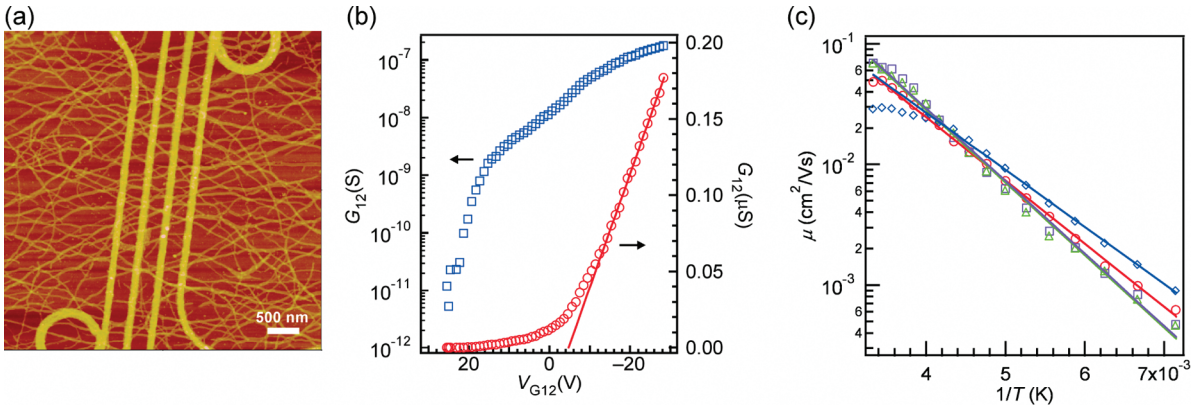

Figure 2. (a) P3BT nanofibers bridging four-probe electrodes (scale bar, 500 nm). (b) Transconductance $G_{12} = (I_D/V_{12})$ of P3OT nanofibers as a function of gate voltage V_{G12} at 290 K. (c) Field-effect mobilities of P3AT nanofibers plotted as a function of inverse temperature, T^{-1}, P3BT (red, circle); P3HT (purple, square); P3OT (green, triangle); P3DT (blue, diamond). Solid lines are the best fits given by an Arrhenius-like behavior: $\mu = \mu_0 e^{-(E_a/k_BT)}$.

kinetically comparable to the self-organization of P3HT but is likely to be much faster than that of P3AT with its longer alkyl chains. The rapid evaporation of a casting solvent may freeze the motion of polymer chains before self-organization is completed and thus prevent the formation of a well-ordered microstructure,[4g] particularly for P3OT and P3DT. In the case of very thin films (2−6 nm), solvent evaporation occurs so rapidly that self-organization cannot be completed, even for P3HT. Thus, a device with a very thin P3HT layer shows as low a mobility as $0.5-1.1 \times 10^{-5}$ cm^2/(V s).[8] By contrast, P3AT nanofibers form gradually in solution during slow cooling of the solution, which results in a well-organized microstructure as revealed with XRD, independent of the alkyl chain length.[3c] Casting a nanofiber solution does not offer the in situ self-organized formation of P3AT molecules into a nanofiber, but the overlying nanofiber layer assembles into a network. Indeed, all P3AT nanofibers have a similar network morphology as illustrated in Figure 1a, and therefore, give a high mobility for all P3ATs despite its small thickness (~3−4 nm).

To characterize the nanofiber network, we used wide-gap electrodes with a spacing (36 μm) much larger than the typical length of the nanofibers (several micrometers). Thus, the resulting carrier transport inevitably involves two processes: carrier transport (i) in a isolated nanofiber and (ii) between nanofibers. We further investigated the carrier transport in isolated nanofibers by using narrow-gap electrodes with a spacing (250 nm) much shorter than the length of the nanofibers, which completely excludes carrier transport between nanofibers. We used a lower solution concentration (0.010 wt %) to decrease surface coverage by nanofibers. Owing to the low coverage, each nanofiber was definitely resolved in the AFM images. Typically, 40−120 isolated nanofibers bridged the electrodes (Figure 2a). With the use of the narrow-gap electrodes, no saturation behavior was obtained in the I_D-V_D characteristics due to the limitation of drain voltage. Thus, the transconductance $G_{12} = (I_D/V_{12})$ was measured as a function of the four-probe gate voltage V_{G12} in the linear regime, G_{12} increased with negative V_{G12} larger than −10 V (Figure 2b). The field-effect mobility of isolated nanofibers, μ_{12}, was determined using the four-probe method described in eq 3.[9] The four-probe method eliminates the contact resistance effect on μ_{12}, which is accompanied by small contact area of isolated nanofiber.[4a,b] Table 2 summarizes field-effect transistor characteristics of isolated nanofibers. As in the nanofiber network, alkyl chain length has little influence on the μ_{12} of isolated nanofibers, despite some variation in the mobility values. The μ_{12} values reach as high as $3.3-6.4 \times 10^{-2}$ cm^2/s, which is comparable to the higher mobility of P3HT nanofibers reported previously and 3−6 times higher than the μ_{linear} of the respective nanofiber network. The carrier transport in a isolated nanofiber is much better than that between nanofibers, strongly indicating the existence of a potential barrier between nanofibers.

Table 2. Field-Effect Transistor Characteristics of Isolated Nanofibers[a]

	μ_{12} (cm^2/s)	V_{T12} (V)	V_{ON} (V)	I_{ON}/I_{OFF}
P3BT	4.9×10^{-2}	−15.6	9.6	2×10^3
P3HT	6.4×10^{-2}	−11.3	15.3	4×10^3
P3OT	6.1×10^{-2}	−4.8	23.1	8×10^3
P3DT	3.3×10^{-2}	−3.7	16.5	6×10^3

[a] Field-effect mobility μ_{12} was determined in the linear regime using eq 3,[9]

$$G_{12} = \left(\frac{I_D}{V_{12}}\right) = \frac{W_{four}^{ef}}{L_{four}} C_{ox}\mu_{12}(V_{G12} - V_{T12}) \quad (3)$$

$$V_{12} = V_2 - V_1$$

$$V_{G12} = V_G - (V_2 + V_1)/2$$

where G_{12} is the transconductance, V_{T12} is the threshold voltage, L_{four} is the electrode spacing, and W_{ef}^{four} is the effective width of the four-probe electrode, $W_{ef}^{four} = Nw_{av}$.

We further measured temperature-dependent $I_D - V_G$ characteristics of nanofiber networks and I_D-V_{G12} characteristics of isolated nanofibers in the temperature range 140−300 K. I_D decreased with decreasing temperature, falling to the background level below 100−140 K. The mobility is determined in the linear regime and plotted as a function of temperature (Figure 2c and Figure S3 in the Supporting Information). In the case of both the nanofiber network and isolated nanofibers, the temperature dependence of the mobility exhibits an Arrhenius-like behavior: the mobility values relate exponentially to the inverse of temperature, T^{-1}. Activation energy values, E_a, determined from the slope of the linear fits to the $\ln\mu - T^{-1}$ plot, are listed in Table 3. The nanofiber network except for P3OT mostly gives slightly higher E_a than the respective isolated nanofibers, suggesting that the energy barrier of carrier transport between fibers is slightly higher than in a fiber. The E_a values are comparable to or slightly larger than the ones reported previously for P3HT nanofibers.[4a,b]

Salleo and co-workers have investigated carrier transport in a fiber and between fibers and proposed that fiber-to-fiber grain boundaries act as large transport barriers compared with the grain boundary in a fiber.[10] In their system, the nanofiber was fabricated by using a directional crystallization method, where the polymer backbone of P3HT was oriented along the fiber

Table 3. Activation Energy of Field-Effect Mobility in Nanofiber Networks and in Isolated Nanofibers

	E_a (meV)	
P3AT	nanofiber network	isolated nanofiber
P3BT	114	104
P3HT	122	119
P3OT	112	120
P3DT	101	94

direction. In contrast, the P3AT nanofiber investigated here consists of a stack of polymer backbones oriented perpendicular to the fiber direction. Here, we consider the possible cause of the potential barrier based on the microstructure of a nanofiber fabricated by using the whisker method illustrated in Figure S1 in the Supporting Information. A nanofiber consists of stacks of extended polymer chains along the fiber direction. The extended polymer chain delocalizes π electrons along the chain. The periodic stacks of the polymer backbone forms a straight pathway for carrier transport along the fiber direction owing to the large overlap between the π electrons. When a carrier moves from one fiber to another at an intersection of fibers, the transport pathway is discontinued by alkyl chains acting as an insulating layer, which contributes greatly to the potential barrier to carrier transport between fibers.

In conclusion, we investigate field-effect carrier transport characteristics of the poly(3-alkylthiophene) nanofiber, focusing on the effect of the alkyl side chain length. In contrast to thin film devices reported previously, where alkyl chain length had a large influence on device performance and longer alkyl chains dramatically reduced the mobility, the present nanofiber devices all give mobilities above 0.01 $cm^2/(V\ s)$, little influenced by alkyl chain length in both nanofiber networks and isolated nanofibers. These high mobilities result from the well-organized microstructure of the nanofiber, which offers a straight pathway of carrier transport along periodic stacks of the polymer backbone, independent of the alkyl chain length. We further investigate the device performance of isolated nanofibers and nanofiber networks. The carrier transport in a isolated nanofiber is better than that between nanofibers, strongly indicating the existence of a potential barrier between nanofibers. On the basis of the nanofiber microstructure, we can conclude that alkyl side chains block the straight pathway, which contributes to the potential barrier to carrier transport between fibers.

Acknowledgment. This work was partly supported by a Grant-in-Aid for Scientific Research (S) (No. 20221005), Scientific Research (B) (No. 20350102), Young Scientists (B) (No. 21740312) and a Grant-in-Aid on Priority Area "Soft Matter Physics" (No. 21015014) from the Ministry of Education, Culture, Sports, Science and Technology (MEXT), Japan.

Supporting Information Available: Experimental procedures, structural parameters of P3AT nanofibers, schematic of a P3AT nanofiber, field-effect transistor characteristics of the nanofiber network at 290 K, I_D-V_G characteristics of nanofiber networks measured in the 140−300 K range, field-effect mobility in the linear regime as a function of inverse temperature, and AFM images of the P3AT nanofiber network. This material is available free of charge via the Internet at http://pubs.acs.org.

References and Notes

(1) (a) Briseno, A. L.; Mannsfeld, S. C. B.; Jenekhe, S.; Bao, Z.; Xia, Y. *Mater. Today* **2008**, *11*, 38–47. (b) Lim, J. A.; Liu, F.; Ferdous, S.; Muthukumar, M.; Briseno, A. L. *Mater. Today* **2010**, *13*, 14–24. (c) Aleshin, A. N. *Adv. Mater.* **2006**, *18*, 17–27. (d) Aleshin, A. N.; Lee, H. J.; Park, Y. W.; Akagi, K. *Phys. Rev. Lett.* **2004**, *93*, 196601. (e) Aleshin, A. N.; Lee, H. J.; Jhang, S. H.; Kim, H. S.; Akagi, K.; Park, Y. W. *Phys. Rev. B* **2005**, *72*, 153202. (f) Hu, W. P.; Nakashima, H.; Furukawa, K.; Kashimura, Y.; Ajito, K.; Torimitsu, K. *Appl. Phys. Lett.* **2004**, *85*, 115. (g) Rahman, A.; Sanyal, M. K. *Phys. Rev. B* **2007**, *76*, 045110.

(2) (a) Martin, C. R. *Science* **1994**, *266*, 1961–1966. (b) Bjørnholm, T.; Hassenkam, T.; Greve, D. R.; McCullough, R. D.; Jayaraman, M.; Savoy, S. M.; Jones, C. E.; McDevitt, J. T. *Adv. Mater.* **1999**, *11*, 1218–1221. (c) Maynor, B. W.; Filocamo, S. F.; Grinstaff, M. W.; Liu, J. *J. Am. Chem. Soc.* **2002**, *124*, 522–523. (d) Zhang, X.; MacDiarmid, A. G.; Manohar, S. K. *Chem. Commun.* (*Cambridge, U.K.*) **2005**, 5328–5330. (e) Liu, J.; Sheina, E.; Kowalewski, T.; McCullough, R. D. *Angew. Chem., Int. Ed.* **2002**, *114*, 329–332. (f) Liu, H.; Reccius, C. H.; Craighead, H. G. *Appl. Phys. Lett.* **2005**, *87*, 253106. (g) Samitsu, S.; Shimomura, T.; Ito, K.; Fujimori, M.; Heike, S.; Hashizume, T. *Appl. Phys. Lett.* **2005**, *86*, 233103. (h) Kim, D. H.; Park, Y. D.; Jang, Y.; Kim, S.; Cho, K. *Macromol. Rapid Commun.* **2005**, *26*, 834–839.

(3) (a) Ihn, K. J.; Moulton, J.; Smith, P. *J. Polym. Sci. Polym. Phys.* **1993**, *31*, 735–742. (b) Kiriy, N.; Jähne, E.; Adler, H. J.; Schneider, M.; Kiriy, A.; Gorodyska, G.; Minko, S.; Jehnichen, D.; Simon, P.; Fokin, A. A.; Stamm, M. *Nano Lett.* **2003**, *3*, 707–712. (c) Samitsu, S.; Shimomura, T.; Heike, S.; Hashizume, T.; Ito, K. *Macromolecules* **2008**, *41*, 8000–8010. (d) Samitsu, S.; Shimomura, T.; Ito, K. *Thin Solid Films* **2008**, *516*, 2478–2486. (e) Samitsu, S.; Takanishi, Y.; Yamamoto, J. *Macromolecules* **2009**, *42*, 4366–4368. (f) Oosterbaan, W. D.; Vrindts, V.; Berson, S.; Guillerez, S.; Douhéret, O.; Ruttens, B.; D'Haen, J.; Adriaensens, P.; Manca, J.; Lutsen, L.; Vanderzande, D. *J. Mater. Chem.* **2009**, *19*, 5424–5435. (g) Liu, J.; Arif, M.; Zou, J.; Khondaker, S. I.; Zhai, L. *Macromolecules* **2009**, *42*, 9390–9393.

(4) (a) Merlo, J. A.; Frisbie, C. D. *J. Polym. Sci. Polym. Phys.* **2003**, *41*, 2674–2680. (b) Merlo, J. A.; Frisbie, C. D. *J. Phys. Chem. B* **2004**, *108*, 19169–19179. (c) Chang, J.-F.; Sun, B.; Breiby, D. W.; Nielsen, M. M.; Sölling, T. I.; Giles, M.; McCullogh, I.; Sirringhaus, H. *Chem. Mater.* **2004**, *16*, 4772–4776. (d) Torrent, M.-M.; Boer, D. Der.; Hadley, P.; Schenning, A. P. H. J. *Nanotechnology* **2004**, *15*, S265–S269. (e) Yang, H.; Shin, T. J.; Yang, L.; Cho, K.; Ryu, C. Y.; Bao, Z. *Adv. Funct. Mater.* **2005**, *15*, 671–676. (f) Zhang, R.; Li, B.; Iovu, M. C.; Jerreries-El, M.; Sauvé, G.; Cooper, J.; Jia, S.; Tristram-Nagle, S.; Smilgies, D. M.; Lambeth, D. N.; McCullough, R. D.; Kowalewski, T. *J. Am. Chem. Soc.* **2006**, *128*, 3480–3481. (g) Kim, D. H.; Jang, Y.; Park, Y. D.; Cho, K. *J. Phys. Chem. B* **2006**, *110*, 15763–15768.

(5) (a) Bao, Z.; Feng, Y.; Dodabalapur, A.; Raju, V. R.; Lovinger, A. J. *Chem. Mater.* **1997**, *9*, 1299–1301. (b) Kaneto, K.; Lim, W. Y.; Takashima, W.; Endo, T.; Rikukawa, M. *Jpn. J. Appl. Phys.* **2000**, *39*, L872–L874. (c) Babel, A.; Jenekhe, S. A. *Synth. Met.* **2005**, *148*, 169–173. (d) Babel, A.; Jenekhe, S. A. *J. Phys. Chem. B* **2003**, *107*, 1749–1754. (e) Zen, A.; Saphiannikova, M.; Neher, D.; Asawapirom, U.; Scherf, U. *Chem. Mater.* **2005**, *17*, 781–786. (f) Park, Y. D.; Kim, D. H.; Jang, Y.; Cho, H. J.; Hwang, M.; Lee, H. S.; Lim, J. A.; Cho, K. *Org. Electron.* **2006**, *7*, 514–520.

(6) Oosterbann, W. D.; Bolsée, J.-C.; Gadisa, A.; Vrindts, V.; Bertho, S.; D'Haen, J.; Cleij, T. J.; Lutsen, L.; McNeill, C. R.; Thomsen, L.; Manca, J. V.; Vanderzande, D. *Adv. Funct. Mater.* **2010**, *20*, 792–802.

(7) DeLongchamp, D. M.; Vogel, B. M.; Jung, Y.; Gurau, M. C.; Richter, C. A.; Kirillov, O. A.; Obrzut, J.; Fischer, D. A.; Sambasivan, S.; Richter, L. J.; Lin, E. K. *Chem. Mater.* **2005**, *17*, 5610–5612.

(8) Sandberg, H. G. O.; Frey, G. L.; Shkunov, M. N.; Sirringhaus, H.; Friend, R. *Langmuir* **2002**, *18*, 10176–10182.

(9) Chen, C. Y.; Kanicki, J. *IEEE Electron Device Lett.* **1997**, *19*, 340–342.

(10) Jimison, L. H.; Toney, M. F.; McCulloch, I.; Heeney, M.; Salleo, A. *Adv. Mater.* **2009**, *21*, 1568–1572.